Nuclear Instruments and Methods in Physics Research A 333 (1993) 153–166
North-Holland

NUCLEAR
INSTRUMENTS
& METHODS
IN PHYSICS
RESEARCH
Section A

An experiment to study CP violation in the B system using an internal target at the HERA proton ring

W. Hofmann

Max-Planck-Institut für Kernphysik, D 6900 Heidelberg 1, Germany

Using the HERA proton beam striking an internal wire target, sufficient numbers of B mesons are produced to allow a search for CP violation in B decays with a sensitivity $\Delta\sin(2\beta) \approx 0.05$, provided that the detector can accept and separate multiple interactions per bunch crossing. This report summarizes our present views concerning the layout of the target, of the spectrometer, and of the trigger system, which selects events containing J/ψ candidates.

1. Introduction

One of the fundamental features of the standard model is the violation of CP symmetry, as observed in the kaon system. Neutral B mesons provide one of the few other systems in nature, where CP violation might be observable, allowing stringent tests of the consistency of the standard model description of the mechanisms of CP violation. B mesons are most easily studied in high-luminosity e^+e^- colliders. Despite the great interest in the particle physics community, it is unlikely that such a machine can be realized in Europe in the near future.

As an alternative, and to allow a continuation of the successful B-physics program carried out at DESY using the DORIS storage ring, a group of physicists centered around the ARGUS collaboration got interested in hadron accelerators as a prolific source of B hadrons. The group [1] is presently studying the option of a major B-physics experiment to be performed at the HERA proton storage ring in fixed target mode using an internal target. Basic goal of the experiment is the detection of CP violation in the "gold plated" $B^0 \to J/\psi\, K_s$ decay mode, using a dedicated detector triggered on lepton pairs from J/ψ decays. With an expected CP asymmetry between B^0 and $\overline{B^0}$ decays as high as $\sin(2\beta) \approx 0.5$ (fig. 1) [2], the experiment is designed to reach an ultimate precision of $\Delta\sin(2\beta) \approx 0.05$, providing a certain safety margin. Besides the central issue of CP violation, the experiment will of course be able to cover many other aspects of B physics, such as lifetime measurements and the study of b-quark production mechanisms. A detailed description of the physics and of the experiment is given in the Letter of Intent submitted to DESY in October 1992 [3]; the summary presented here is based on this document, with emphasis on more recent work concerning in particular the tests of the internal target and the triggering scheme.

The main characteristics of proton–nucleus interactions resulting in B production are summarized in fig. 2: at the primary interaction vertex, a pair of b particles is produced together with about ten other fast tracks and a number of low-energy nuclear fragments. At beam energies around 1 TeV, a B meson will have a median flight path of about 7 mm. For decays into $J/\psi\, K_s$, with $J/\psi \to e^+e^-$ or $\mu^+\mu^-$, the leptons have a median momentum around 40 GeV. The kaon with a median momentum of 50 GeV decays into pions in the 20 GeV momentum range. Because of the Lorentz boost, the decay particles are confined to the forward hemisphere and are in most cases contained in the cone 10 mrad $< \theta <$ 200 mrad, which corresponds to a 90% solid angle coverage in the center-of-mass of the reaction. One measures the time-dependent CP asymmetry between B^0 and $\overline{B^0}$ decay rates to $J/\psi\, K_s$,

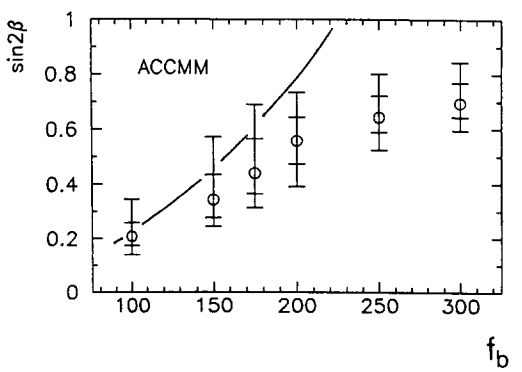

Fig. 1. Best fit results for the expected size of the CP asymmetry $\sin(2\beta)$ as a function of f_b ($B_b = 1$ assumed) [2a]. Also shown is the analytic form of Bigi [2b].

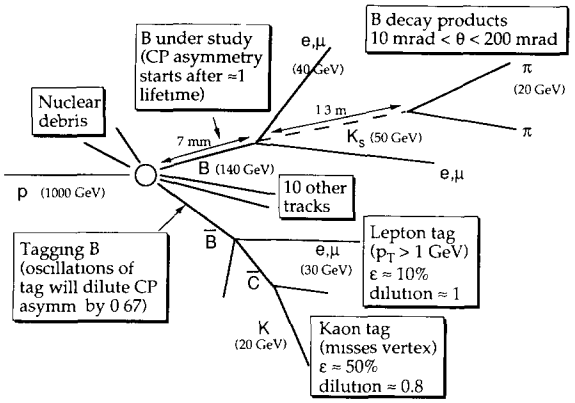

Fig 2. Typical features of B hadron production in proton–nucleus interactions at 1 TeV. Indicated is the typical (median) momentum of particles, and the median decay length.

$A = \sin(xt)\,\sin(2\beta)$. Here, $x = \Delta M/\Gamma \approx 0.67$ characterizes the B^0–$\overline{B^0}$ flavor oscillations, and t is the decay time measured in units of the B lifetime. As the asymmetry A is modulated with a term $\sin(xt)$, events where the B meson decays after less than one mean lifetime do not contribute significantly to the CP violation measurement. Therefore, rather stringent cuts on vertex separation can be used without increasing the statistical error of the measurement of $\sin(2\beta)$.

Since the decay mode $B^0 \to J/\psi\, K_s$ leads to a CP eigenstate, one cannot tell from the final state whether one is observing a B^0 or $\overline{B^0}$ decay. For the measurement of a CP asymmetry between B^0 and $\overline{B^0}$ decays, the initial flavor of the decaying B has to be tagged by other means. For the proposed experiment, we studied tagging based on either the charge of leptons from the semileptonic decay of the second B in the event, or based on the charge of kaons from the decay of this second B. After a cut in the transverse momentum of the lepton, $p_T > 1$ GeV, in order to remove wrong-sign leptons from the $b \to c \to l + X$ cascade, semileptonic decays provide a rather clean tag, albeit with low ($\approx 10\%$) tagging efficiency. In contrast, kaon tags have a higher tagging efficiency, since most B decays contain at least one charged kaon, but mistagging is more frequent, resulting in a dilution of the observable CP asymmetry. For either tag, an additional dilution is introduced by flavor mixing of the tagging B before its decay. Averaged over all species of tagging B mesons, these oscillations reduce the net CP asymmetry by about a factor 0.65–0.70.

The statistical error in the determination of the CP asymmetry $\sin(2\beta)$ is then given by $\Delta\sin(2\beta) \approx (1/D)(K/N)^{1/2}$, where N is the number of tagged events surviving a vertex separation cut (in our case, at 0.7 lifetimes), $D \approx 0.5$ is the net dilution factor, and $K \approx 1.5$ is a cut-dependent statistical factor arising from the average over the time-dependent CP asymmetry. To achieve a statistical error in $\sin(2\beta)$ of 0.05, one needs roughly 3000 events. To relate this number of tagged B decays to the total number of interactions required, we need to account for the ratio of the b cross section to the total cross section ($\approx 10^{-6}$ for a nuclear target) [4,5], for the probability to generate a B^0 or $\overline{B^0}$ in a b event (≈ 0.8), for the B^0 branching ratio to $J/\psi\, K_s$ ($\approx 4 \times 10^{-4}$), for the leptonic J/ψ branching ratio (≈ 0.14) and for the $K_s \to \pi^+\pi^-$ branching ratio (0.69), resulting in roughly 3×10^{-11} decays per event. Including estimates for the peak reconstruction efficiency (0.5), the trigger efficiency (0.7), the effect of various cuts (0.5) and the tagging efficiency (0.5), we find that the search for CP violation requires about 10^{15} interactions, corresponding to 5 years of data taking at a 20 MHz interaction rate. For the proposed experiment, we aim for rates in the 30–50 MHz range. Given that the bunch crossing rate at HERA is only 10 MHz, these numbers imply that the detector has to be able to handle and sort out multiple events in each bunch crossing.

Obviously, such an experiment represents quite a technical challenge; at higher energies, with larger b cross sections, the task would be simplified considerably. However, compared to machines like LHC or SSC the HERA ring has a big advantage: it is available now and it can accommodate a dedicated B experiment (in contrast, e.g, to the Tevatron collider, where all suitable interaction regions are occupied). HERA will be operated more or less continuously for many years, and has a unity duty cycle. These two factors provide a significant gain relative to fixed-target programs at CERN or FNAL. Finally, the high intensity of the internal beam allows the use of a thin line-target, with negligible re-interactions. A B experiment running at rates as high as 50 MHz would use 2×10^{11} p/h, corresponding to a beam lifetime of 100 h at the nominal HERA current. Such a lifetime limit introduces only a negligible degradation in the integrated luminosity for e–p collider operation, as required for the parasitic operation of the experiment. The remainder of this paper will address some of the most crucial points of the experiment:

- the efficient operation of the internal target;
- the detector, which shares many features with SSC/LHC detectors;
- the trigger and readout scheme;
- the rejection of backgrounds under the B signal.

2. The internal target

Two options were studied for the internal target in the HERA proton ring: a gas jet target in the beam

core, and a halo target, acting essentially like a collimator. The gas jet target has the advantage that it represents a well-established technique. However, the high interaction rate requires a dense target, which will, integrated over a run, increase the beam emittance. To minimize this emittance growth $\Delta\epsilon$ due to multiple scattering in the target, $\Delta\epsilon = \beta\theta_{\text{rms}}^2$, a small β-function at the location of the target is required. On the other hand, one needs to create a large interaction volume, to have the multiple interaction vertices in each bunch crossing separated by distances large enough to allow an unambiguous vertex assignment of tracks. A transverse spread of the vertices is most efficient, given that particle distributions are strongly peaked in the forward direction, but such a large beam size is in direct contradiction with the low-β requirement.

In contrast, a halo target acting like a collimator uses only protons in the machine halo, which are diffusing outwards towards the aperture limit. A halo target making use of these protons does not interfere with the beam emittance, or with the luminosity operation. It is well known that only the edges of a collimator are illuminated; such a target will therefore provide a line source, where two coordinates of the vertices are known with high precision (some 10 μm), and where vertices are spread out in the third (transverse) direction, along the collimator edge. The difficulty with such a target is that is needs to intercept a significant fraction of all protons being lost in the machine; a target with 50% efficiency (i.e., capturing 50% of all protons being lost) will require beam lifetimes below 50 h to sustain a 50 MHz interaction rate. Since our simulations indicate that such efficiencies can be achieved with a properly designed target, we adopted a halo target made of multiple thin wires or ribbons as our primary choice. (Wires are used instead of a solid collimator block in order to avoid secondary interactions in the target and to provide a well-defined location of the vertex in the beam direction.)

The layout of the halo target is shown in fig. 3; it consists of two sets of four steel wires of about 50 μm effective diameter. The two sets are separated along the beam by about 5 cm. The position of each wire is remotely controlled; typically, the wires will be positioned at 4 standard deviations from the beam, corresponding to about 2 mm. The three to five interaction vertices per bunch crossing will be spread uniformly over the eight wires, and over distances of several mm along each wire, minimizing track confusion between vertices. The thin wires provide well-defined vertex lines. To be used as an efficient constraint on the B production point, the wire (or ribbon) dimensions should be smaller than the experimental resolution on the B decay vertex (which is around 20–30 μm rms in the transverse direction, and 300–400 μm along the beam). The main difference between this system and a real collimator is that a particle has to cross a wire a few hundred to thousand times before it is absorbed.

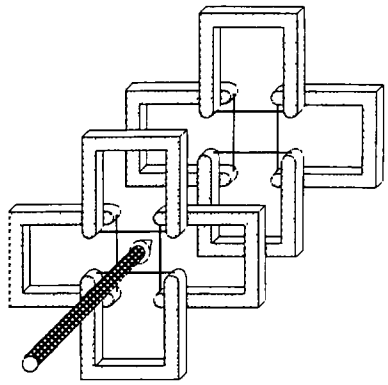

Fig. 3. Layout of the wire target geometry.

As pointed out earlier, it is crucial that the target is very effective in catching protons about to be lost in the machine. The target efficiency is governed mainly by the competition of the halo target with other aperture limitations in the machine. Once the betatron amplitude of a particle is large enough that it intersects one of the target wires, the following processes compete:

- absorption in the target wire;
- increase of the betatron amplitude due to stochastic diffusion and loss of the particle due to the finite aperture of the machine;
- increase of the betatron amplitude due to multiple scattering in the target wire itself, resulting in the loss of the particle.

In addition, the energy loss in the target wire causes synchrotron oscillations of the halo particles. Contrary to first rough estimates, however, detailed tracking simulations showed that the influence of these synchrotron oscillations on the target efficiency is negligible.

At 4σ from the beam, the diffusion speed is expected to be of the order of 0.1σ/s, increasing steeply with the distance from the beam [6,7]. Therefore, a particle at 4σ will usually last only a few seconds before reaching the effective aperture of 6σ to 7σ. During these few seconds, the particle has to cross enough wire material to be absorbed with a high probability. For given wire dimensions, this is most easily achieved for dense targets with high atomic number.

The emittance increase due to multiple scattering, $\Delta\epsilon = \beta\theta_{\text{rms}}^2$, is governed by the local β-function and by the ratio of the radiation length to the nuclear interaction length of the target. On average a particle traverses one interaction length before being absorbed, resulting in

$$\theta_{\text{rms}} = 14\ \text{MeV}/\text{p}(\lambda_{\text{int}}/\lambda_{\text{rad}})^{1/2}.$$

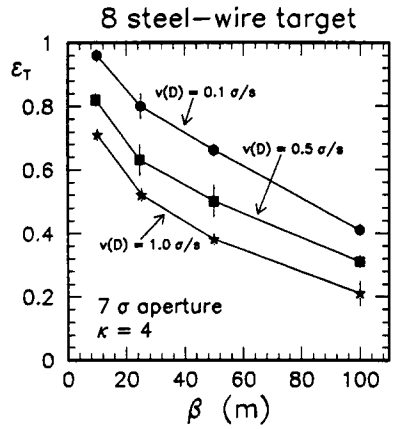

Fig. 4. Absorption efficiency of the multiwire target of fig. 3 as a function of the β-function for a 7σ aperture of the machine and several choices of the drift speed $v(D)$.

To minimize the losses due to multiple scattering in the target, a small β-function and a low-Z target are needed.

As a compromise between these conflicting requirements, we initially considered iron or copper as target materials. More recently, we became aware of the large numbers of highly ionizing nuclear fragments produced in such targets. Therefore, lighter targets such as aluminum or carbon are now favored, since a significant fraction of the slow tracks will penetrate the first layers of the silicon vertex detector and may cause significant radiation damage.

The efficiency of the target was studied extensively by tracking simulations and by beam dynamics calculations based on the diffusion equation [8]; in addition, a series of experimental measurements was conducted during the last year. Some results of the simulations are summarized in figs. 4 and 5. In fig. 4 the expected dependence of the target efficiency on the β-function is illustrated, for different values of the diffusion speed (the upper curve with a speed of $0.1\sigma/s$ is probably most realistic). As expected, a high target efficiency is

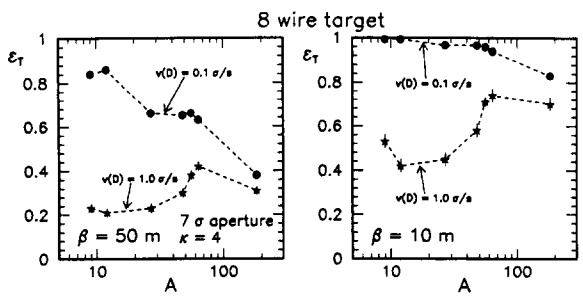

Fig. 5. Absorption efficiency as a function of the atomic mass number A of the target for a 7σ aperture and two choices of $v(D)$ and two values of β.

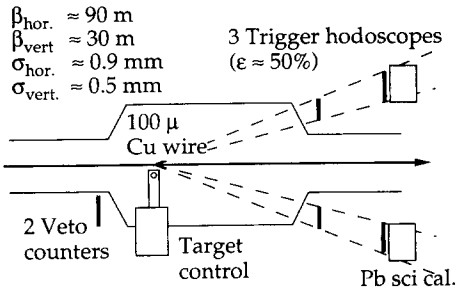

Fig. 6. Test setup with a single-wire internal target in the HERA proton ring.

obtained with small β-functions (for reference, the e–p experiments have β-functions of about 1 m (vertical) and 10 m (horizontal) at the IR). Fig. 5 shows the dependence of the target efficiency on the target mass number A, for a $\beta = 10$ m and of $\beta = 50$ m. The latter value is considered as the upper limit acceptable for the experiment. In the case of moderate diffusion speeds, low-A targets are preferred, and reach efficiencies exceeding 80%.

In order to establish a firmer basis for these estimates, a target test setup was installed near the HERA west hall, and was operated with beam for about 10 h during the 1992 running period. The setup consisted of a (vertical) 100 μm copper wire mounted on a standard collimator drive, of three trigger hodoscopes at small angles downstream of the target wire, and of two veto counters upstream (fig. 6). The relevant horizontal β-function at the location of the wire was 90 m, somewhat larger that ideal. In addition to the rates of the counters, beam parameters such as current and lifetime as well as the background rates in the big e–p experiments were monitored.

Typical results of a test run are illustrated in fig. 7; shown are the wire position as a function of time – the wire is moved towards the beam in steps of 30 μm – and the counting rates in the scintillator hodoscopes. After each step of the wire, the counting rate shows a steep rise, followed by a gradual settling of the rates. The step arises when the wire clears a new region of phase space from halo particles; the rate then settles towards an equilibrium between outward diffusion of the particles and absorption at the wire. Also shown is the fraction of events where the upstream veto counters fired. It is obvious that the increased counting rate is really due to interactions in the target wire, rather than due to a general disturbance of the beam resulting in an increased halo: before the wire is moved into the beam, about 90% of the events have the upstream veto counters set, indicating that these events are caused by particles lost all around the machine, and creating showers in the beam pipe and the magnets upstream of the target. With the target in the beam,

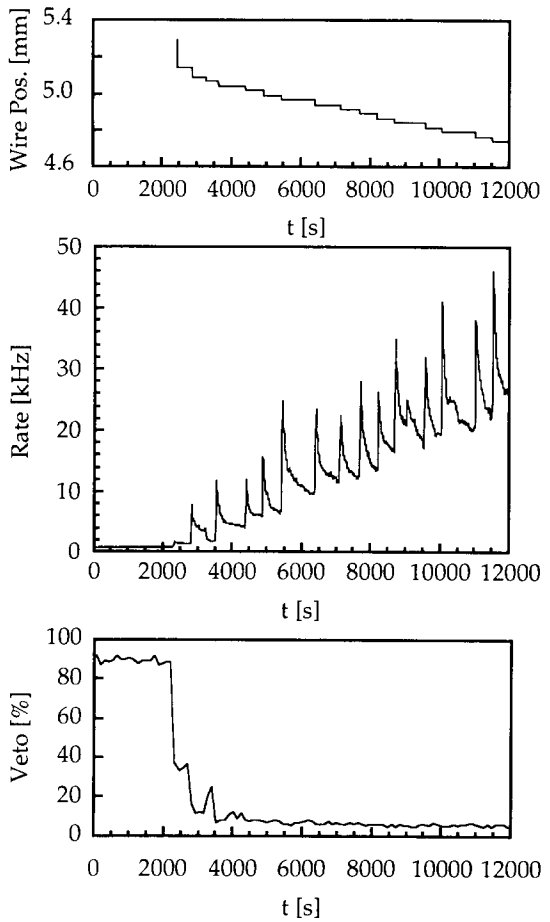

Fig. 7. Results of a test of the wire target. Top: wire positions as a function of time. The beam size is roughly 1 mm. Middle: corresponding counting rate in the scintillator hodoscopes downstream of the target. Bottom: fraction of events where the veto counters upstream of the wire target fired.

the veto rate decreases to about 5%, thereby excluding upstream particle losses as a dominant source of the hodoscope counting rate. In fact, the timing spectra of the veto counters indicate that with the wire target in the beam, most of the remaining veto counts result from backwards moving nuclear fragments created in interactions at the target wire. During this wire test, the backgrounds monitored in the ZEUS experiment did not increase (see fig. 7).

Fig. 8 shows another test run, where the target was moved at a slower pace and where the settling of counting rate after each step of the target wire is obvious. Here and in all other tests, the HERA machine was operated at about 1% of the design current, carried by a ten bunch train. The observed rates extrapolate to MHz rates for the design current; peak rates measured in the test were in the 100 kHz range, equivalent to about 10 MHz at design current. From

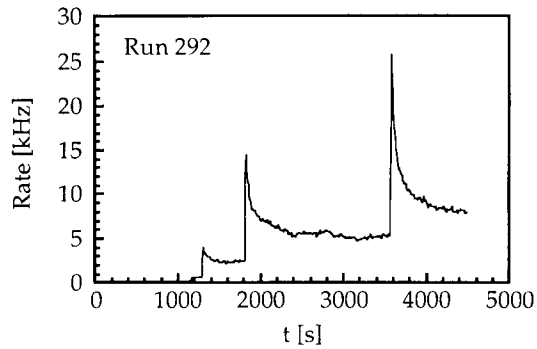

Fig. 8. Counting rate in the scintillator hodoscopes as a function of time. The wire target was moved towards the beam in three steps.

the measured beam lifetime and the machine currents, the loss rate can be calculated and hence the fraction of particles absorbed in the target wire. The resulting target efficiencies are in the range of a few percent (fig. 9), with peak efficiencies of 15% in some runs. While these efficiencies are significantly lower than the ones required for the actual experiment, the efficiency values are well reproduced by our simulations (fig. 9). The main reasons for the low efficiency are the fact that we used only one instead of eight target wires, that the wire was installed in a location with a quite large β-function, and that during these runs the effective aperture of about 5σ was smaller than expected, due to obstacles and misalignments in the HERA proton ring.

For the next running period, the test setup will be upgraded using thicker wires with a total mass corresponding to the eight-wire target, with a second (hori-

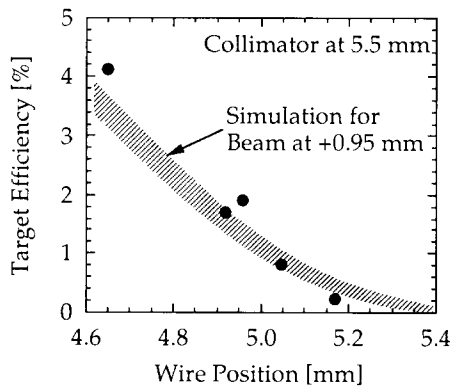

Fig. 9. Target efficiency (calculated using the machine current, the beam lifetime and the counting rate and efficiency of the hodoscopes), as a function of the position of the wire target. The band indicates the results of Monte Carlo tracking simulations; since the absolute position of the target relative to the beam was not calibrated, the curves were shifted by about 1 mm for the best fit.

zontal) wire, with large-acceptance triggering and veto counters, with a tracking system to track particle trajectories to the wire target, and with an improved data acquisition system. The configuration should allow absorption efficiencies close to the final requirements, and will allow a much more detailed evaluation of the quality of our simulations.

3. The detector

The requirements on the detector of the proposed B experiment at HERA can be summarized as follows:
- Reconstruction of multiple events with as many as 50 tracks per bunch crossing at 10 MHz bunch crossing rate with high efficiency;
- reconstruction of B decay vertices;
- identification of leptons and charged kaons;
- fast and highly selective trigger on J/ψ;
- radiation-hard detector elements.

The detector concept discussed here is based on the work presented in the Letter of Intent [3]; while we expect the general concept to survive without major modifications, numerous changes concerning the optimization of individual detector components are under discussion.

The low B production cross section requires the efficient detection of decay products; therefore, the detector has to cover most of 4π in the center-of-mass frame. Fig. 10 displays the geometrical acceptance for $B^0 \to J/\psi\, K_s$ decays as a function of the minimum and maximum polar angle covered by the detector. In the detector design, we aimed for a polar angle coverage of roughly 10 to 200 mrad, corresponding to 90% of 4π in the cms. Lower angles are excluded because of the proton beam pipe going through the detector; an acceptance significantly larger than 200 mrad would result in drastically increased costs for the spectrometer

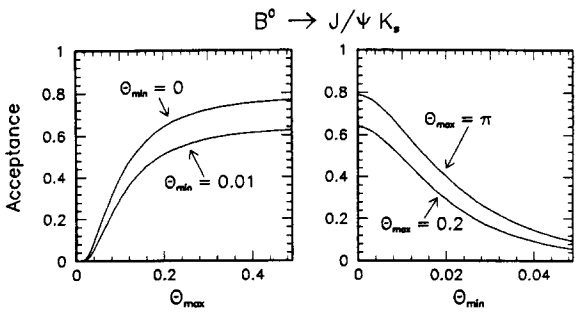

Fig. 10. Geometrical efficiency of the detector for $B^0 \to J/\psi\, K_s$ decays as a function of the maximum polar angle covered by the detector (left), and as a function of the minimum polar angle (right). Included is the efficiency for the detection of the K_s, which has to decay before the magnet.

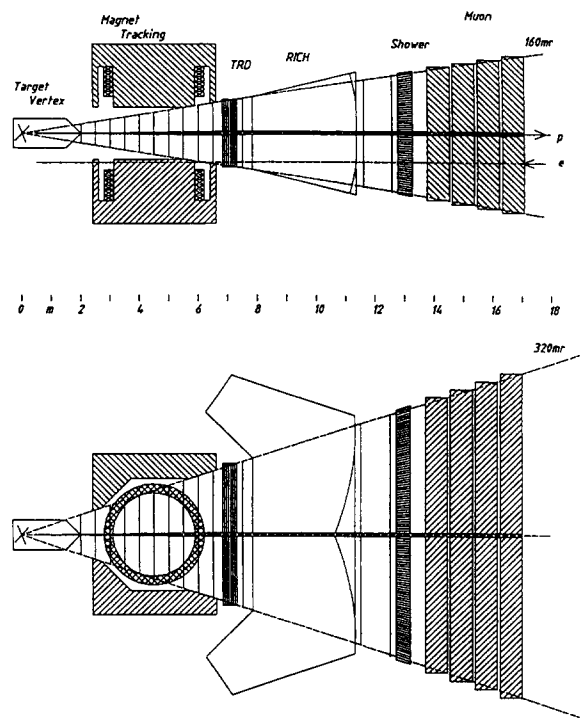

Fig. 11. Configuration of the proposed B spectrometer, with the silicon vertex detector, the main tracking system with a dipole magnet, TRD and RICH counters for particle identification, the electromagnetic calorimeter and the muon system.

magnet. The plots in fig. 10 are made for a single-magnet spectrometer, with the magnet centered about 4 m downstream from the target. The efficiency of such a spectrometer is limited to about 80% even in the case of perfect angular coverage because the K_s is required to decay upstream of the analysis magnet. The position of the magnet (for a fixed magnet aperture) represents a compromise between solid-angle coverage and K_s acceptance. In principle, this compromise can be circumvented by two-magnet systems as the ones proposed by the LHB [9] and COBEX [10] groups; there, a first magnet provides large solid-angle coverage and a second magnet analyzes most of the late decays of fast K_s. We have analyzed such configurations; their main disadvantage for the application in HERA is the increased total length of the spectrometer, which is difficult to fit into the available hall. Given this length constraint, we found that two-magnet solutions did not result in significant gains in acceptance.

The preliminary design of the detector is shown in fig. 11. A 2 m long vertex detector system is followed by the analysis magnet packed with tracking chambers, a TRD for electron identification, an imaging Cherenkov counter for kaon identification, the electromagnetic (spaghetti) calorimeter and the muon system.

Interleaved between TRD, RICH and calorimeter are further tracking chambers, mainly for triggering purposes. The spectrometer covers about 165 mrad in the non-bending plane and about 300 mrad in the bending plane. Note that the HERA electron ring has to go through the detector and through the pole face of the magnet, at a distance of about 90 cm from the proton beam. One particularly crucial point is the design of the beam pipe in the very forward direction; normal straight beam pipes or conical pipes result in a large number of secondary interactions in the pipe, with reaction products that are swept into the detector if the interactions occur before or inside the magnet. At this time, we are considering composite beam pipes made of a series of inverse cones. Such geometries limit the minimum angle between a particle and the beam pipe wall to about 50 mrad, and reduce the number of secondary interactions. A (GEANT-)simulated event with three simultaneous proton–nucleus interactions is shown in fig. 12, demonstrating the high density of tracks particular in the forward region.

The high density of tracks places serious restrictions on the choice of tracking detectors. For strip detectors, such as silicon strip counters, gas microstrip, or drift chambers, the maximum allowable readout pitch is severely limited by the maximum tolerable occupancy. Fig. 13 shows the maximum pitch as a function of the inner radius of the detector, for a peak occupancy of 5–10% per detector cell. (In the region of the rapidity

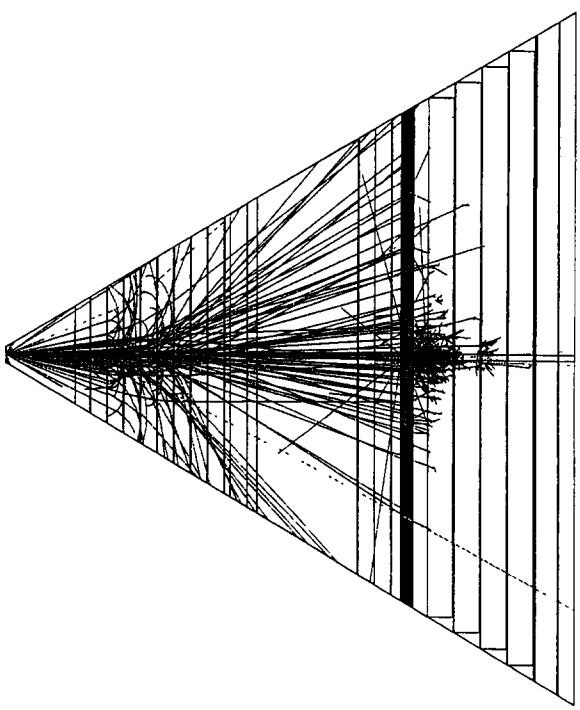

Fig. 12. Simulated event with three simultaneous interactions.

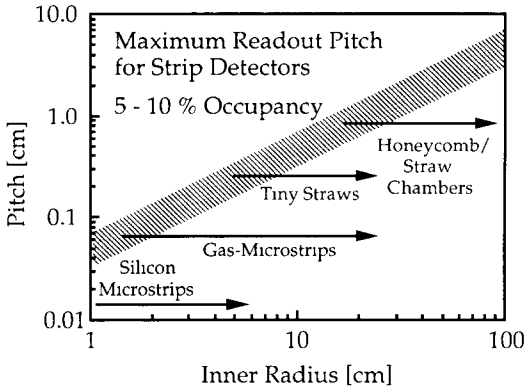

Fig. 13. Maximum allowable readout pitch for strip detectors, assuming a peak occupancy of 5 to 10%, as a function of the inner radius of the corresponding tracking system.

plateau, it can be shown that the particle density is only a function of the distance from the beam, irrespective of the distance from the target [3].) At the innermost radius of the tracking system – we aim for 1 cm – only silicon systems can be used. The intermediate region from about 5 to 30 cm would be ideally suited for gas microstrip counters; for the outer regions, conventional drift chambers or straw chambers can be used. If gas microstrip counters cannot be demonstrated to work on the time scale of this experiment, small-cell drift chambers or tiny straw chambers would provide an alternative, together with a slightly enlarged silicon tracker.

A particularly crucial component of the detector is the silicon vertex detector system, which consists of a series of 15 planes (perpendicular to the beam) of double sided silicon strip counters, supplemented by stereo layers. The counters are arranged with progressive distances to provide a uniform coverage in rapidity. For the measurement of CP asymmetries, the requirements on this silicon system are rather modest; its most critical task is the rejection of background from events with pair production of charmed quarks, where both charms decay semileptonically and where the resulting pair of charged leptons falls into the J/ψ mass range. Cuts based on kinematics, invariant masses, and event topology are not sufficient to fully suppress this background. The vertex detector provides the important additional constraint that the two leptons have to form a common vertex consistent with the trajectory of the B candidate. Since the contributions to the vertex resolution from multiple scattering are proportional to the inner radius of the detector, we aim for an inner radius of 1 cm. Each single plane of silicon detectors will not cover the full aperture of the spectrometer, but rather end at about 6 cm from the beam. In total, each track has six to seven hits in the silicon system. Since a larger beam clearance is needed for

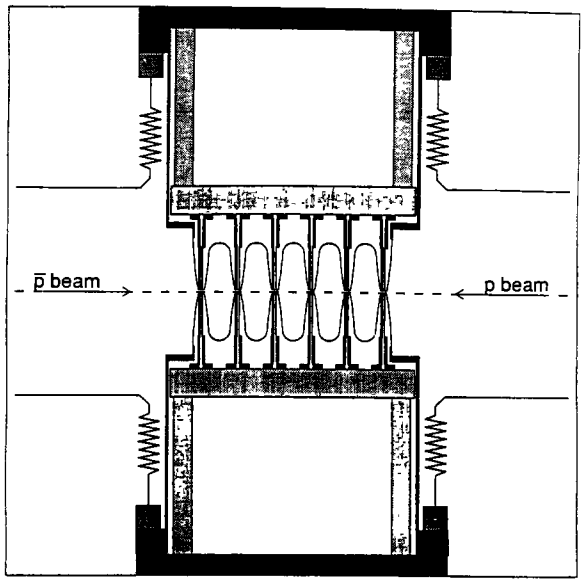

Fig. 14. Sketch of the detector assembly and the "Roman pots" used at the SPS. The system consists of six equidistant detector planes. The inner rf shields are at a distance of 1.5 mm from the beam. The detector mounting plates are attached to the vacuum bulkheads. The bellows allow pot movements in the vertical direction

injection, the whole silicon system will be retractable, similar to the Roman pot assemblies used successfully in long-term tests of a similar, albeit smaller system at the CERN-SPS collider [11] (fig. 14). This detector system will measure track impact parameters with errors of about 30 μm. Simulations down to the level of individual strip signals, and including pattern recognition, show that a high track reconstruction efficiency can be maintained even in bunch crossings with as many as 100 tracks in the detector.

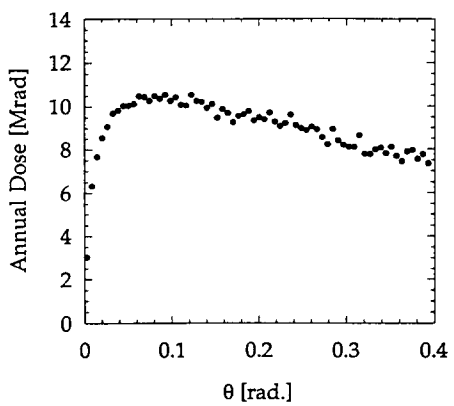

Fig. 15. Annual radiation dose deposited at the inner edge of the silicon counters ($r = 1$ cm), as a function of the polar angle.

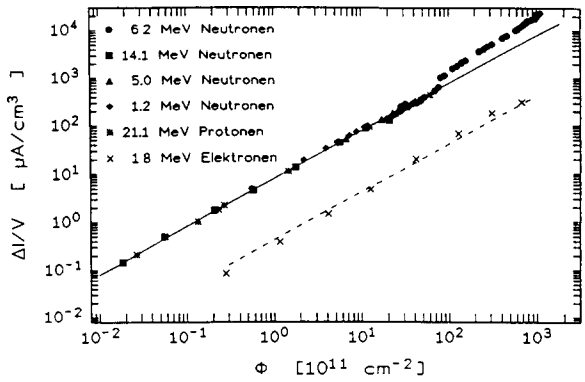

Fig. 16. Leakage current measured for silicon diode detectors as a function of the equivalent flux of 1 MeV neutrons [13]. The radiation damage by 1 MeV neutrons is roughly equivalent to the damage by charged relativistic hadrons; 10 Mrad correspond to a flux of 3×10^{14} particles/cm^2.

The inner edges of the silicon detectors are exposed to very high radiation doses. As shown in fig. 15, peak doses are about 10 Mrad/yr. Radiation damage in silicon detectors is the subject of intensive research regarding in particular the applications at SSC and LHC, and the effects of radiation damage are reasonably well understood. They include [12,13]:

– An increased bulk leakage current, proportional to the integrated dose. The leakage current I_1 results in a higher shot noise,

$$Q_{\text{noise}} = (I_1 T_1/e)^{1/2} \sim (AWT_1)^{1/2},$$

where A is the area of one strip, W is the thickness of the waver and T_1 is the integration time constant of the preamplifier. Fig. 16 shows the measured volume leakage current of a typical silicon diode as a function of radiation dose [13]. Using short strips and fast shaping (50 ns or less), a sufficient signal-to-noise ratio is possible even at doses near 10 Mrad, corresponding to 3×10^{14} particles /cm^2.

– The trapping of charge carriers, resulting in a reduced collection efficiency. Present measurements indicate, however, that even for doses in the range of several Mrad, collection efficiencies of 70–90% can be reached [13].

– Charge trapping in oxide layers, resulting in potential shifts or breakthrough. These effects can be minimized by careful choice of the geometry and of the operating potentials.

– Creation of additional acceptor sites, causing a p^+nn^+ silicon detector to convert into a p^+pn^+ detector, with the p–n junction moving to the opposite side of the detector (fig. 17) [13]. This type inversion occurs quite early, at fluxes of a few 10^{12} particles/cm^2, but the detectors continue working after the inversion. The main limitation is simply that with increasing acceptor

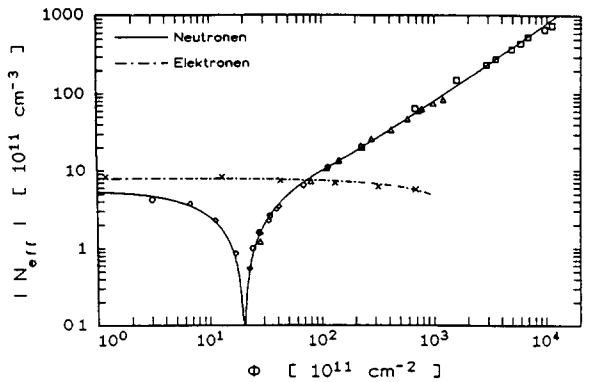

Fig. 17. Net impurity concentration in silicon as a function of the equivalent integrated flux of 1 MeV neutrons, determined from the voltage required for full depletion of the detector [13]. Initially, the detector could be fully depleted by applying 80 V bias voltage; at the peak flux, about 350 V were required.

concentration, higher voltages are required to fully deplete the detector. Doses up to several Mrad seem feasible from this point of view.

Generally, for the whole tracking system and the TRD we plan to use packets of tracking devices with multiple and redundant layers, each packet providing three or more stereo views.

The RICH system uses a C_5F_{12} radiator, and is designed to provide a 3σ particle separation up to 100 GeV/c momentum. It is read out by TMAE activated CsI photocathodes. A simulated RICH image is shown in fig. 18. Despite the high density of rings in the central region, the Monte Carlo simulations show low

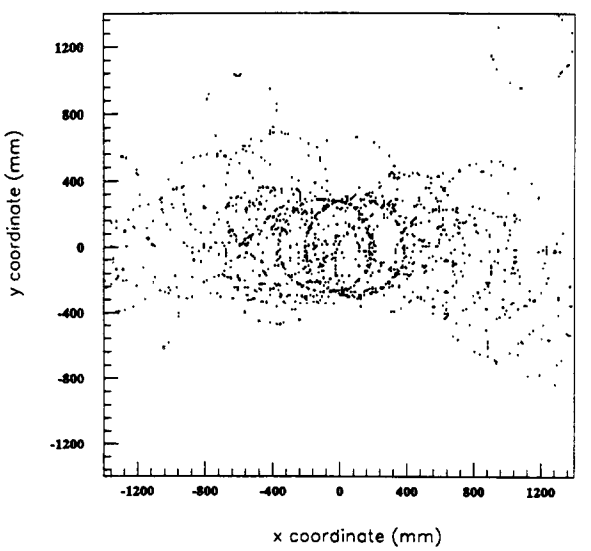

Fig. 18. Typical RICH image for a bunch crossing with multiple interactions.

misidentification probabilities in the range of 1%, well within the requirements for efficient kaon tagging. More recently, we have also studied C_4F_{10} as a radiator gas; its improved transparency for UV photons compared to C_5F_{12} promises a significant (> 50%) gain in the number of detected photons.

The calorimeter serves mainly as an electron identifier and fast trigger element; its performance in terms of energy resolution is not very critical. However, the high particle density near the beam pipe requires a design with a minimal Molière radius to reduce shower overlap, and with the possibility for a fine-grained readout. A spaghetti calorimeter seems to be the most suitable device [14,15].

The requirements for the muon tracking system are quite relaxed compared to the front end tracking. The muon filter consists of 3 to 4 m of iron (more in the core region), interleaved with drift chambers with cell sizes of about 1 cm, with fast CF_4-based gases to provide drift times well below the bunch crossing frequency of 100 ns.

4. Readout and trigger

The readout and trigger system is a multilevel system modeled after the systems designed for LHC and SSC detectors (fig. 19). In total, about half a million of front-end channels have to be handled. Following suitable input elements (preamplifiers, shapers, time-to-voltage converters), the signals will be clocked into a 60–120 element first level pipeline, to provide 6–12 μs time for the first-level trigger decision. The first-level pipeline will most likely be realized as a switched-capacitor array. The first-level trigger, also pipelined, selects di-lepton candidates with invariant masses above 2.5 GeV; its trigger rate is expected in the 10–50 kHz range. Most recent analog pipelines are read out by multiplexing the signals of the typically 32–128 channels per chip onto a single fast ADC, thereby avoiding excessive cabling between the front-end electronics and the data acquisition hardware. In usual designs, the first-level pipeline has to be stopped during the readout. In our application, the resulting dead time is problematic, in particular if the first-level trigger rate is higher than expected. Therefore, we have to use a modified readout scheme of the first-level pipeline, which does not introduce extra dead time. This can be achieved either by implementing independent read and write pointers, as in the HARP design [16], or by adding a secondary storage array, which again needs to feature independent read/write access.

After the first level pipeline, data are digitized, preprocessed by fast digital signal processors, and stored in a second-level digital pipeline, awaiting the second level trigger signal to arrive after 200–500 μs.

The second level trigger should make use of the vertex information for lepton candidates, and refine the cuts on particle identification; we expect the second level trigger to provide a factor 10 reduction in rate, resulting in peak trigger rates around 5 kHz. Following the second-level trigger, an event builder with 50–250 MBytes/s throughput should route the signals to a third level trigger farm. The required computing power is estimated to about 5000 VAX/780 equivalents, or 50 of presently available workstations. This third level trigger will provide a full track fit for J/ψ candidates and should allow another factor of 10 reduction in event rate, with a final tape-writing speed of less than 500 events/s, or about 10 MBytes/s. We feel that essentially all elements of this readout system exist today; the evolution in the next years will however allow considerable cost savings compared to similar systems installed now.

The most critical part of the trigger system is the first-level trigger, which selects and reconstructs di-lepton candidates. Lepton candidates identified in the calorimeter or the muon system define a "region of interest" in the tracking chambers behind the magnet. Hit data in these regions of interest are analyzed to check for tracks and to determine their momentum. Up to 10 to 15 lepton candidates need to be processed in parallel. For all pair candidates, invariant masses are computed and compared to a trigger threshold. A few 10^8 mass combinations have to be calculated per second, which seems feasible either using memory look-up tables or fast DSPs. For the track finding step, two techniques are considered. One option is to switch the tracker data in a region of interest to conventional pattern matching units, which compare in a partly serial, partly parallel fashion the hit pattern to sets of predefined masks. About 10^{11} masks need to be processed per second, which represents an increase in complexity of about one order of magnitude compared to existing trigger processors as the one used e.g. in ARGUS. A problem with this approach is the huge amount of data that is moved between the readout system and the trigger processor. A more elegant solution [17] is to map the chamber data onto arrays of relatively simple processors, each of which is responsible for a certain area of a tracking chamber and holds all the relevant hit data. For a lepton candidate, estimated track parameters are passed to the appropriate processor(s) in the nearest chamber in front of the calorimeter and muon system. If the processor finds a matching hit in the data, it refines the track information and passes the message to the relevant processors in the next chamber, and so on. If more than one matching hit is found, the processor issues multiple messages. The whole system acts basically like a Kalman filter, successively refining track parameters (and rejecting bad candidates), until final track parameters are obtained from the processors in the first trigger chamber right behind the magnet. The chamber areas will be mapped onto processors in a way to provide a uniform load; since a processor may receive multiple messages concerning track candidates, it needs to be equipped with input and output buffers and will use an internal processing pipeline. The main advantage of this second scheme – on which present efforts are centered – is that only the relatively modest information concerning track candidates has to be moved through the system, rather than the full chamber data. Preliminary simulations indicate that the trigger system needs to process about two muon candidates and four electron candidates per bunch crossing. Detailed

Table 1
Dilepton sources and backgrounds. All cross sections refer to e^+e^- or $\mu^+\mu^-$ production in single pN collisions. In the calculation of backgrounds due to particle misidentification, a 1% misidentification probability per hadron is assumed. In events with multiple interactions, misidentified hadrons from different interactions can combine to form a fake di-lepton. The total fake rate is therefore proportional to the square of the number of interactions per event.

Source	Cross section within ± 50 MeV around the J/ψ mass	Cross section for dilepton masses > 2.5 GeV	Tracks come from primary vertex?	Tracks form common vertex?
$B \to J/\psi K_s$	≈ 0.6 pb	≈ 0.6 pb	N	Y
$B \to J/\psi X$	≈ 25 pb	≈ 25 pb	N	Y
Semileptonic B decays	≈ 2 pb	≈ 50 pb	N	N
Semileptonic charm decays	≈ 1.5 nb	≈ 30 nb	N	N
Direct J/ψ production	≈ 30 nb	≈ 30 nb	Y	Y
Drell–Yan	≈ 0.15 nb	≈ 3 nb	Y	Y
Particle misidentification for $p_t > 0.5$ GeV/c	$\approx 0.7\,\mu$b ≈ 100 nb	$\approx 15\,\mu$b $\approx 2\,\mu$b	Y	Y

Table 2
Rate estimates for $B^0 \to J/\psi K_s$.

bb production rate	$40\ s^{-1}$ for $p_{beam} = 820$ GeV ($70\ s^{-1}$ for $p_{beam} = 1000$ GeV)
$b\bar{b} \to b\bar{d}$	0.8
$B^0 \to J/\psi K_s^0$	4×10^{-4}
$Br(J/\psi \to l^+ l^-) Br(K_s^0 \to \pi^+ \pi^-)$	0.1
Average geometrical and reconstruction efficiency	0.33
Trigger efficiency	0.7
Lepton quality cuts	0.75
Vertex cut	0.50
Kinematical cuts	0.65
15000 h running time	5.4×10^7 s
Number of events	3900 for $p_{beam} = 820$ GeV (6800 for $p_{beam} = 1000$ GeV)

GEANT-based trigger simulations and studies of the data flow in the trigger system are in progress. Table 1 summarizes the sources of real or fake di-lepton candidates at the trigger level; by far the dominant source of triggers are fake muons due to decays in flight or punchthrough, and fake electrons due to overlap of photons and charged tracks in the calorimeter.

5. Expected performance of the experiment

The various factors and efficiencies involved in the detection of $B^0 \to J/\psi K_s$ decays are summarized in table 2; for 15000 h of running time we expect about 4000–7000 reconstructed decays, depending on the energy of the HERA proton ring, which could ultimately run at energies as high as 1 TeV. Table 3 summarizes the various factors contributing to the flavor tagging and the CP violation measurement. Tagging efficiencies and mistagging probabilities are based on ARGUS measurements of kaon and lepton production in B decays. As already mentioned in the introduction, the lepton tag provides a rather clean sample, but low efficiency, whereas the kaon tag has a high tagging efficiency, but also a significant fraction of wrong tags. Combining the two tagging techniques, a resolution of $\Delta\sin(2\beta) \approx 0.065$ at 820 GeV beam energy appears feasible. For 1 TeV beam energy, the resolution improves to $\Delta\sin(2\beta) \approx 0.050$ due to the higher B cross section. This statistical error compares favorably with the expected size of the effect (see fig. 1). Systematic errors in the determination of the CP asymmetry may arise, e.g., from unequal production rates of B^0 and $\overline{B^0}$, and are addressed in detail in ref. [3]; basically, one will use reference processes such as the $B^0 \to J/\psi K^*$ decay to check for experimental biases.

A final question to be addressed is the background under the $J/\psi K_s$ signal, and its influence on the CP

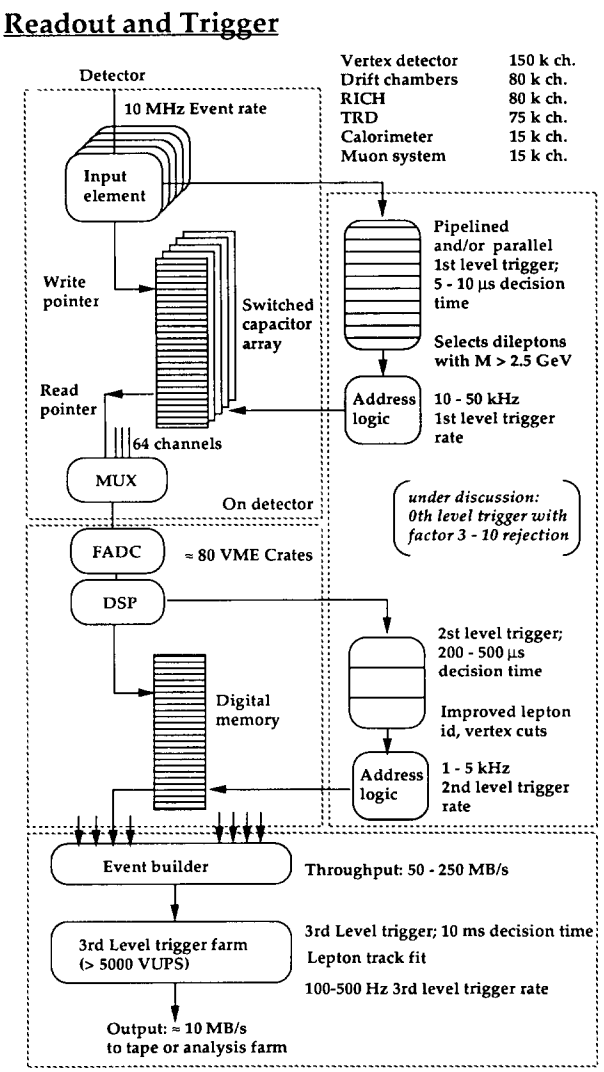

Fig. 19. Data acquistion system with first and second level pipelines and the first, second, and third level trigger processors.

Table 3
Tagging efficiencies and dilution factors.

	Lepton tag	Kaon tag
Cuts in impact parameter	none	$\sigma > 2$ SD $\sigma < 1$ mm
Cuts in momentum	$p > 5$ GeV/c $p > 0.7$ GeV/$c \times \theta^{-0.85}$ $p_t > 1$ GeV/c	$p > 4.5$ GeV/c $p < 50$ GeV
Geometrical acceptance	82%	83%
Detection efficiency after cuts	55%	55%
Probability c to detect correct sign tag from B^0 or B^+ (including mixing)	9.6%	24.7%
Probability w to detect wrong-sign tag from B^0 or B^+ (including mixing)	2.0%	5.6%
Probability f to detect fake tag	3.1%	22.1%
Total tagging efficiency $c + w + f$	14.7%	52.4%
Tagging dilution $(c - w)/(c + w + f)$	0.52	0.36
Number of tagged events (for $p_{beam} = 820$ GeV/c)	570	2040
Error in sin 2β	0.11	0.08
Combined error in sin 2β	0.065	

measurement. Cuts to enhance the signal-to-background ratio include momentum cuts on the leptons (5–20 GeV, depending on the polar angle), roughly equivalent to cuts in the lepton transverse momentum at about 0.5 GeV. This cut strongly suppresses fake leptons due to misidentification of low-p_T pions or due to photon conversion, and leptons from charm decays. Of course, the di-lepton and di-lepton-K_s masses have to be consistent with the J/ψ mass and the B mass, respectively, within the experimental resolutions of 10 and 14 MeV. One then requires a well-separated secondary vertex of the two leptons, consistent with the trajectory of the B candidate. The secondary vertex is typically reconstructed with a precision of 300–400 μm along the beam and of 25 μm in the transverse direction, and an 8σ separation is required between the main vertex and the secondary vertex. Finally, cuts are applied to the decay angles of the J/ψ and of the B; combinatorial backgrounds tend to peak in the forward and backward directions, whereas the real signals have a roughly uniform distribution.

Table 4
Detector requirements of the B experiment compared to standard LHC detectors. Compared are the time intervals T between bunch crossings, the particle densities dn/dy in the central rapidity region, the number of interactions per crossing, the dependence of the annual particle flux on the distance R from the beam as well as the flux at the inner radius r_{min} of the detector.

	HERA-B	LHC
T	96 ns	15 (25?) ns
dn/dy	2 – 4 (H) (Fe)	6–7
Interactions per crossing	3–5	> 15
Particle flux per year	$2\times10^{14}/R^2$ [cm^2]	$6\times10^{15}/R^2$
Particle flux at r_{min}	2×10^{14}/cm^2 at 1 cm	6×10^{13}/cm^2 at 10 cm

The backgrounds can be separated into two major categories: backgrounds due to genuine di-leptons combined with some K_s in the event, and backgrounds involving fake leptons. Genuine di-leptons can either arise from B decays, or from charm decays. In the first case, we find a S/B ratio in excess of 100, in the second case we obtain $S/B \approx 10$. Another source of di-leptons is direct J/ψ production by gluon fusion. These di-leptons come from the main vertex and are easily rejected; according to our simulations, the S/B due to this process is well above 10. Backgrounds with one real lepton from a charm or b decay, combined with a fake lepton, turn out to be negligible compared to those with two genuine leptons, simply because in such events the probability for a semileptonic decay of the second heavy quark is large compared to the misidentification probability. Finally, after a full analysis, backgrounds from two fake leptons are down by a factor 30 compared to the signal; such leptons tend to have either very small impact parameters (if a track from the primary vertex is mis-identified as a lepton), or rather large impact parameters in case of conversions or decays in flight. In either case, the secondary-vertex fit rejects the event.

Finally, our studies indicate [3] that the CP violation measurement is surprisingly insensitive to backgrounds under the signal; even S/B ratios around unity are tolerable. The reason is simply that, as far as the CP signal is concerned, even most of the genuine events in the B peak are "background" in the sense that they have, e.g., a bad tag because of mixing of the tagging B. Additional background underneath the peak is irrele-

vant, unless it becomes comparable to this "intrinsic" background.

6. Technical feasibility of the experiment

To judge the technical feasibility of this challenging, but potentially extremely rewarding experiment it is instructive to compare the requirements with those of LHC experiments. In table 4 some of the relevant quantities, such as the time between bunch crossings (relevant for the bandwidth of the front-end systems), the particle density per unit of rapidity, the number of interactions per crossing, the particle flux at fixed detector radius and the peak particle flux at the innermost radius are contrasted. The conclusion is that in all but one respect, the B detector is intermediate between existing detectors and LHC detectors; the one exception is the flux and the radiation damage of the innermost detectors. However, in the B detector, this innermost silicon system is small and relatively inexpensive; one can afford to replace it once per year, and always have a spare assembly prepared. Because of the fixed target geometry of the experiment, such an exchange should be relatively simple.

In many areas, the proposed experiment will try to build upon the R&D for the LHC. A number of groups work on related topics, such as RD-2 (Tracking/Preshower), RD-6 (Tracking TRD), RD-10 (Radiation-Hard Gaseous Detectors), RD-11 (Second-Level Triggering), RD-20 (Silicon Strip Detectors) and RD-21 (Collider Beauty Physics). Contacts (so far mostly at an informal level) exist with many of the groups, and we envision a close cooperation in the development of the detector components and the readout electronics.

7. Summary

CP violation is generally viewed as one of the most fundamental issues in particle physics and merits strong and continuing efforts. The detection of CP violation in the B system appears within reach of a fixed-target experiment at HERA. Such a dedicated B physics experiment could operate parasitically using an internal target and would not interfere significantly with the normal e–p luminosity operation of the machine.

The design of the detector is clearly very challenging, but it can exploit the enormous amount of R&D work under way for the LHC. With one exception – the issues of radiation damage in the innermost few cm of the detector – the basic performance parameters of the detector are relaxed compared to full-scale LHC detectors, and the system can to a large extent be realized based on existing technology.

The most important R&D issues to be addressed include
- the rate capability of the internal target;
- the detailed design of the trigger processor;
- the issues of radiation hardness;
- the efficiency of the charged-particle tracking system and of the pattern recognition software, related to the granularity and redundancy of the chambers.

Work is in progress in all of these areas and will hopefully culminate in the submission of a technical proposal to DESY some time in 1993. In an optimistic scenario, major components of the detector could be installed and ready for data taking early in 1997. We are open for the participation of interested groups, contributing to the design and construction of the detector on this relatively tight time scale.

References

[1] Authors of the Letter of Intent: H. Albrecht, H. Kapitza, O. Mai, H. Schröder, H.D. Schulz, R. Wurth: DESY, Hamburg; H. Kolanoski, R. Mankel, B. Spaan: Institut für Physik, Univ. Dortmund; R. Mundt, T. Oest, R. Reiner, W. Schmidt-Parzefall: II. Inst. für Experimentalphysik, Univ. Hamburg; W. Hofmann, S. Khan, K.T. Knöpfle, T. Lohse, M. Seeger, M. Spahn, J. Spengler: MPI für Kernphysik, Heidelberg; V. Pugatch: Inst. for Nuclear Research, Kiew; V. Cindro, G. Kernel, P. Križan, E. Križnič, M. Starič: Inst. J. Stefan and Oddelek za fiziko, Ljubljana; R. Männer, F. Klefenz: Inst. für Informatik, Univ. Mannheim; I. Belyaev, M. Danilov, Yu. Gerstein, F. Khasanov, S. Semenov, A. Snijko, I. Tichomirov, Yu. Zaitsev: Inst. of Theoretical and Experimental Physics, Moscow; G. Bohm, S. Nowak, M. Walter: DESY, Zeuthen.

[2a] M. Schmidtler and K.R. Schubert, Z. Phys. C 53 (1992) 347. The values have been updated using the latest CLEO results on b → u transitions (private communication);

[2b] I.I.Y. Bigi, Invited Lecture at the Rencontres de Moriond, Les Arcs, March 1992; UND-HEP-92-BIG01 (1992).

[3] H. Albrecht et al., Letter of Intent, DESY-PRC 92/04 (1992).

[4] P. Nason, S. Dawson and R.K. Ellis, Nucl. Phys. B303 (1988) 607, B327 (1989) 49, B335 (1990) 260.

[5] W. Beenacker et al., Nucl. Phys. B351 (1991) 507.

[6] M. Seidel, The HERA-p collimation system and first experience with a single collimator, Internal HERA note, DESY (1992), and private communications.

[7] L. Burnod, G. Ferioli and J.B. Jeanneret, CERN/SL/90-01 (1990).

[8] D.A. Edwards and M.J. Syphers, AIP Conf. Proc. 184 (1989) p. 2, eds. M. Month and M. Dienes.

[9] T. Nakada, A study of CP-violation in B-meson decays using a gas jet at LHC, Expression of Interest, presented at the General Meeting on LHC Physics and Detectors, Evians les Bains, France, 1992; and
Y. Lemoigne, these Proceedings (Workshop on Beauty

'93, Liblice Castle, near Prague, Czech Republic, 1993) Nucl. Instr. and Meth. A 333 (1993) 113.
[10] A. Brandt et al., CERN-SPSC/88-33 (1989); and S. Erhan et al., these Proceedings (Workshop on Beauty '93, Liblice Castle, near Prague, Czech Republic, 1993) Nucl. Instr. and Meth. A 333 (1993) 101.
[11] J. Ellet et al., Nucl. Instr. and Meth. A317 (1992) 28.
[12] D. Nygren and H. Spieler, in: Radiation Effects at the SSC, ed. M.D.G. Gilchriese, SSC-SR-1035 (1988).
[13] R. Wunstorf, DESY FH1K-92-01 (1992).
[14] D.W. Hertzog et al., Nucl. Instr. and Meth. A294 (1990) 446.
[15] D. Acosta et al., Nucl. Instr. and Meth. A294 (1990) 193, A314 (1992) 431.
[16] RD-2 Collaboration, D. Munday et al., CERN/ECP 92-3 (1992).
[17] S. Weseler, private communication.